

Singlet polaron theory of low-energy optical excitations in NiPS₃

I. J. Hamad,¹ C. S. Helman,² L. O. Manuel,¹ A. E. Feiguin,³ and A. A. Aligia²

¹*Instituto de Física Rosario (CONICET) and Facultad de Ciencias Exactas, Ingeniería y Agrimensura, Universidad Nacional de Rosario, 2000 Rosario, Argentina*

²*Instituto de Nanociencia y Nanotecnología CNEA-CONICET,*

Centro Atómico Bariloche and Instituto Balseiro, 8400 Bariloche, Argentina

³*Physics Department, Northeastern University, Boston, MA 02115, USA*

Light-matter interactions can be used as a tool to realize novel many-body states of matter and to study the interplay between electronic and magnetic degrees of freedom. In particular, tightly bound many-body states that behave as coherent quasi-particles are rare, and may lead to unconventional technological applications beyond the semi-conductor paradigm, particularly if these excitations are bosonic and can condense. Two-dimensional magnetic systems present a pristine platform to realize and study such states. We construct a theory that explains the low-energy optical excitations at 1.476 eV and 1.498 eV observed by photoluminescence, optical absorption, and RIXS in the van der Waals antiferromagnet NiPS₃. Using *ab initio* methods, we construct a two-band Hubbard model for two *effective* Ni orbitals of the original lattice. The dominant effective hopping corresponds to third-nearest neighbours. This model exhibits two triplet-singlet excitations of energy near two times the Hund exchange. From perturbation theory, we obtain an effective model for the movement of the singlets in an antiferromagnetic background, that we solve using a generalized self-consistent Born approximation. These singlet excitations, dressed by a cloud of magnons, move coherently as polaronic-like quasi-particles, “singlet polarons”. Our theory explains the main features of the observed spectra.

I. INTRODUCTION

For many years, the idea of an archetypal two-dimensional (2D) magnetic material was a dream of theorists and experimentalists alike. The physics in low dimensional systems differs in many aspects from the three-dimensional counterpart, mostly due to a more pervasive and dominant role of quantum fluctuations, that prevent spontaneous symmetry breaking and thus, true long range order, from taking place in absence of anisotropy [2]. This offers the possibility of realizing exotic quantum states of matter, such as quantum spin liquids [3]. Still, different types of magnetic order are possible in 2D depending on the interactions and anisotropies present in the system [4–9]. The recent discovery of atomically thin exfoliated van der Waals magnets [4, 5, 10, 11], particularly of the family of MPX₃ metal phosphorous trichalcogenides (M=Mn, Fe, and Ni), has opened the research field in new unexplored and exciting directions, that also have important technological implications.

While many of these compounds are ferromagnets [5], NiPS₃ was found to realize an unconventional zigzag antiferromagnetic order, first observed in its bulk form [12, 13], and also in quasi-2D multi-layer exfoliated structures [10], enabling studies of the dimensional crossover of the magnetic order [8, 14–17]. The minimal model used to understand the magnetic properties of this material consists of a generalized Heisenberg model with spins $S = 1$ sitting in place of the Ni²⁺ ions, at the vertices of a honeycomb lattice [7]. While the low-energy magnetic excitations in NiPS₃ seem to be well described by spin-wave theory [18], this material has been shown to exhibit strong interactions between spin-ordering and

optical excitations [19–25]. In particular, several recent optical experiments [photoluminescence, optical absorption, and resonant inelastic X-ray scattering (RIXS)] [19] identified two very narrow peaks: I at 1.4756 eV and II at 1.498 eV. The width of both peaks decrease with decreasing temperature and for peak I, it reaches 0.4 meV well below the Néel temperature of about 155 K. Increasing temperature, the peaks disappear together with the antiferromagnetic order. Furthermore, the lowest energy peak observed in photoluminescence is accompanied by two much lower intensity satellite peaks.

Due to this unusually narrow width, it has been proposed that peak I [19] corresponds to a condensate of Zhang-Rice singlet (ZRS) excitons [26]. These singlets are low-energy states formed between a hole in the d shell of a transition-metal ion and another in the p shell of an anion (usually oxygen) with the same symmetry. They were widely discussed in the context of the cuprates [26–29]. Peak II has been loosely assigned to a two-magnon sideband associated with peak I.

The interest in these excitation peaks, as well as other structures below the conduction gap, has increased in the last years [8, 16, 21–25, 30–34]. Calculations including correlations are limited to a NiS₆ cluster. They indicate that the ground state is a triplet in a mixed configuration between d^8 and d^9L and the excited state possibly related to peak I is a singlet in the d^9L configuration, compatible with a ZRS [16, 19, 32–34]. However, a detailed description of the singlet, as contained for example in the studies of the cuprates [26–29] has not been presented. In addition, since these studies are limited to one Ni atom, the dynamics of the excitons is not studied.

In this work, we have combined three theoretical approaches to study the electronic structure of the system:

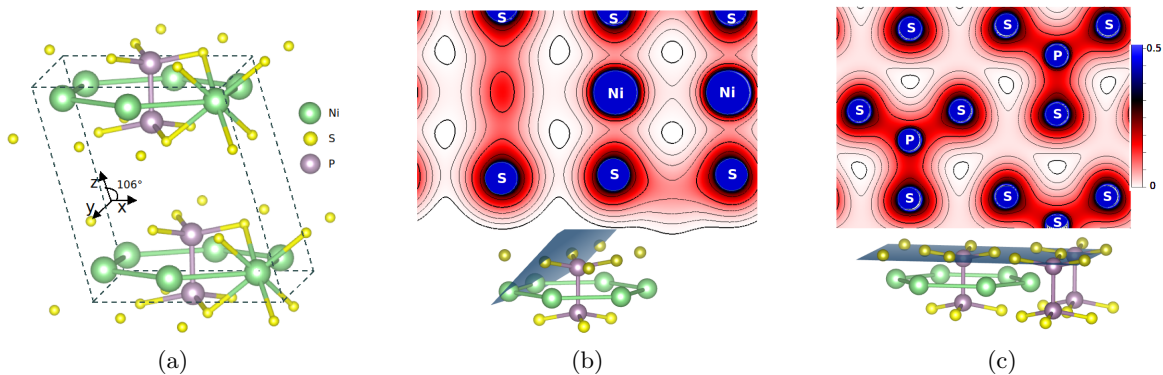


FIG. 1: (Colour online) (a) Structure of bulk NiPS_3 . Note the P dimer bonded to S atoms at the centre of the Ni hexagons. (b) Valence charge density for two different planes as sketched in each case. Note the difference in the charge density along bonds in each case. The colour scale unit is in electrons/ \AA^3 [1].

(i) we construct a low-energy Hubbard model with hopping matrix elements obtained by *ab initio* calculations using maximally localized Wannier functions (MLWFs) in a suitable chosen energy range and standard on-site interactions. We find that two Wannier functions centered at the Ni sites, but containing a mixture of orbitals of other atoms, perfectly fit the bands near the Fermi energy with suitable hoppings. An adequate choice of Wannier functions has been shown to be important in the description of the cuprates [35]. This model leads naturally to two triplet-singlet excitations of energy near $2J_H$ where $J_H \sim 0.75$ eV is the Hund coupling. (ii) From perturbation theory, we construct an effective Hamiltonian H_{eff} that describes the movement of the singlets in a spin-1 antiferromagnetic background. (iii) Finally, we solve H_{eff} using a generalization of the self-consistent Born approximation (SCBA), which is the state-of-the-art technique to tackle similar but simpler problems. Previously, the case of a single exciton moving in Sr_2IrO_4 was mapped to a hole moving in an antiferromagnetic background [36]. However, in the present work we have a spin-1 background and two types of singlet excitations, each of which can transform into the other. Therefore, the theory is considerably richer and more involved.

Our findings indicate that the narrow peaks I and II observed in optical experiments can be attributed to unconventional singlet polaron quasi-particles. These are triplet-to-singlet excitations that become dressed by magnons as they move, causing a distortion in the zig-zag antiferromagnetic order of NiPS_3 . Additionally, we trace the origin of the satellite peaks to strings of misaligned spins.

II. RESULTS

A. Atomic and magnetic structure

The NiPS_3 layered compound belongs to the transition-metal phosphorus trichalcogenides (TMPS₃)

family. In its monolayer form, it adopts a hexagonal structure with the D_{3d} point group, while the bulk form displays a monoclinic structure with the C_{2h} point group, resulting from a stacking of monolayers displaced in the x -direction, as shown in Fig. 1(a). The monolayer has a thickness of 3.18 Å formed by three atomic planes, where the Ni atoms are in the central plane surrounded by two planes of S atoms above and below. Within the planes, the Ni atoms form a hexagonal lattice where each one is bounded to six S atoms and the P atoms are near the centre of the hexagon at the height of the S planes (top and bottom) forming a P dimer. This P dimer is strongly bonded to the S atoms, forming an anion complex with a pyramidal structure. In Fig. 1 (b) and (c), we present valence-charge density obtained by DFT calculation, whereby in comparison, the plane conformed by Ni and S atoms have more localized charge than the plane conformed by S and P atoms, supporting the presence of the anion complex at the centre of the hexagonal lattice.

Since NiPS_3 exhibits a relatively high Néel temperature (155K)[13], the antiferromagnetic phase is stable with strong magnetic interactions. In that phase, the magnetization axis lies along the monolayer. The Ni atoms form ferromagnetic zigzag chains ordered antiferromagnetically between them, as presented in Fig. 2(c). Thus, the magnetic structure reveals that at first and second magnetic nearest neighbors (NNs) the Ni atoms can be either ferromagnetically or antiferromagnetically aligned, while at distances corresponding to third magnetic NNs [the atoms connected by the vectors δ_i in Fig. 2(c)], the correlations are antiferromagnetic. It is likely that the origin of this long-range magnetic interactions lies in the anion complex formed at the centre of the hexagonal lattice that acts as an effective bridge among third NN Ni atoms. These findings are further supported by the results presented in the following section.

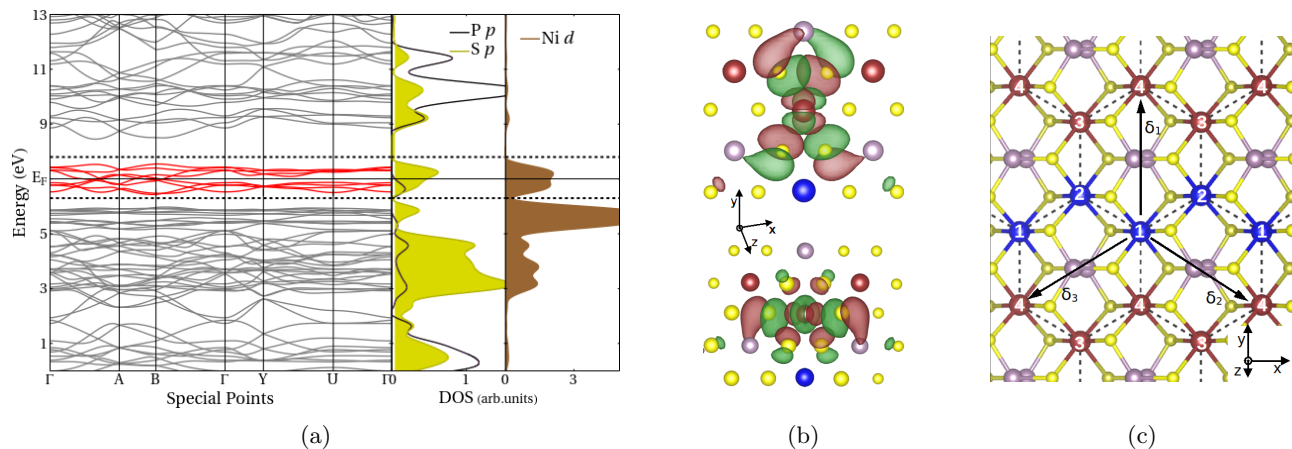


FIG. 2: (Colour online) (a) Band structure of NiPS₃ for the non-magnetic case, with a unit cell that contains four unit formulae. In red, fit of the bands using the MLWFs. Projected density of states on different atom types are shown on the side of the band structure. (b) Representation of the Wannier functions centred on the Ni atoms (depicted as blue/red spheres). The top/bottom panels display the odd/even Maximally Localized Wannier Functions (MLWFs), respectively. It is noteworthy that in both cases, the wave functions extend from the S atoms (yellow spheres) to the P atoms (violet spheres), indicating a strong bonding among them and displaying the mixed nature of each wave function. (c) Top view of the structure planes of NiPS₃, the numbered red/blue spheres are the Ni atoms with spin up/down respectively. The magnetization lies in the zigzag chain direction, which is the x -direction. Yellow/violet spheres correspond to S and P atoms. The δ_i arrows point to the third NN Ni atoms of Ni₁.

B. The effective two-band Hubbard model

We first extract the MLWFs from a non-magnetic density-functional theory (DFT) calculation, including all relevant orbitals in an energy window near 10 eV, obtaining 72 Wannier functions per unit cell. The resulting hopping between Ni and S orbitals is in the range 0.5-0.9 eV, while the corresponding hopping between P and S orbitals is much larger, between 1.5 and 2 eV. This value indicates that P atoms play an important role and cannot be neglected. This is also consistent with the obtained intermediate charges of the atoms, near Ni^{+1.2}, P^{+1.5}, S^{-0.9}. Constructing a low-energy many-body Hamiltonian with this information is very involved and does not allow one to single out the essential ingredients of the problem. Therefore, we followed another strategy successfully used by two of us in another highly covalent system [37]. We took an energy window of 1.5 eV around the Fermi level containing isolated bands, as shown between dashed lines in Fig. 2(a). We obtain two Wannier functions of mixed character centered at each Ni site and an excellent fit of the bands shown as red bands in Fig. 2(a). In the scale of the figure, no difference can be detected between the calculated bands and the fit. Other convergence criteria are also fulfilled as required in Ref. [38].

We find that sites Ni₁ and Ni₃, which are non-equivalent in the full magnetic structure, behave as equivalent in this reduced subspace. The same happens for Ni₂ and Ni₄. Due to the shift of adjacent layers of the material, only one of the lattice vectors is the axis of a

C_2 symmetry (rotation of 180 degrees around δ_1). One of the resulting MLWFs is odd [Fig. 2 (b) top] and the other even [Fig. 2 (b) bottom] under C_2 . We denote them by “ o ” and “ e ”, respectively. The occupancies of both MLWFs are very close to 1 (1.03) as expected for an insulating system in a basis of states with small mixing with excited states.

We denote by δ_1 the vector that points from Ni₁ to its third NN Ni atom Ni₄ [see Fig. 2 (c)] in the direction of a C_2 axis. We call δ_2 and δ_3 the other two vectors that connect third NNs obtained by rotating δ_1 by (neglecting a very small distortion) 120 and 240 degrees, respectively. Surprisingly, the dominant hoppings are those between third NNs. The magnitudes are $t_1 = 0.2247$ eV for two o orbitals at positions differing in δ_1 , and $t_2 = 0.1643$ eV for $e - e$ and $t_3 = 0.1048$ eV for $e - o$, in both δ_2 and δ_3 directions. The next hopping is a NN $o - o$ one in the opposite direction of δ_1 , whose value is -0.0514 eV. Since, as shown below, ultimately the terms governing the dynamics of the excitations are of the order of the square of these hoppings, we start our discussion by retaining for the moment only the third NN hoppings. In this way, the layers of the compound become divided into four independent honeycomb sublattices. Adding the standard interaction for two degenerate d orbitals [39, 40], we obtain the Hubbard model $H_{\text{Hub}} = H_{\text{hop}} + H_{\text{int}}$, with

$$H_{\text{hop}} = \sum_{i \in A, \sigma} [t_1 o_{i+\delta_1, \sigma}^\dagger o_{i, \sigma} + t_2 \sum_{\delta_j \neq \delta_1} e_{i+\delta_j, \sigma}^\dagger e_{i, \sigma}]$$

$$\begin{aligned}
& -t_3 \sum_{\delta_j \neq \delta_1} (-1)^j (e_{i+\delta_j\sigma}^\dagger o_{i\sigma} + o_{i+\delta_j\sigma}^\dagger e_{i\sigma}) + \text{H.c.}], \\
H_{\text{int}} = & \sum_i [U \sum_\alpha n_{i\alpha\uparrow} n_{i\alpha\downarrow} + U' \sum_\sigma n_{i\sigma} n_{i\bar{\sigma}} \\
& + (U' - J) \sum_\sigma n_{i\sigma} n_{i\bar{\sigma}} - J (o_{i\uparrow}^\dagger e_{i\downarrow}^\dagger e_{i\uparrow} o_{i\downarrow} + \text{H.c.}) \\
& + J' (o_{i\uparrow}^\dagger o_{i\downarrow}^\dagger e_{i\downarrow} e_{i\uparrow} + \text{H.c.})], \quad (1)
\end{aligned}$$

where the first sum is over one of the two sublattices (A) of the honeycomb lattice, α denotes the orbitals o or e , $n_{i\alpha\sigma} = a_{i\sigma}^\dagger \alpha_{i\sigma}$ and $\bar{\sigma} = -\sigma$.

The eigenstates and energies of H_{int} at each site are easily determined. In particular, in the most relevant subspace of two particles at site i , they correspond to three singlets $|i\beta\rangle$ and one triplet $|itS_z\rangle$. Explicitly, writing only the triplet of highest projection $S_z = 1$, they are

$$\begin{aligned}
|i a\rangle &= \frac{1}{\sqrt{2}} (o_{i\uparrow}^\dagger o_{i\downarrow}^\dagger + e_{i\uparrow}^\dagger e_{i\downarrow}^\dagger) |0\rangle, \quad E_a = U + J', \\
|i b\rangle &= \frac{1}{\sqrt{2}} (o_{i\uparrow}^\dagger o_{i\downarrow}^\dagger - e_{i\uparrow}^\dagger e_{i\downarrow}^\dagger) |0\rangle, \quad E_b = U - J', \\
|i c\rangle &= \frac{1}{\sqrt{2}} (o_{i\uparrow}^\dagger e_{i\downarrow}^\dagger - o_{i\downarrow}^\dagger e_{i\uparrow}^\dagger) |0\rangle, \quad E_c = U' + J, \\
|it1\rangle &= o_{i\uparrow}^\dagger e_{i\uparrow}^\dagger |0\rangle, \quad E_t = U' - J. \quad (2)
\end{aligned}$$

For spherical symmetry (and approximately in general) $U' = U - 2J$ and $J' = J$. This leads to a triplet ground state, a singlet (a) at energy $4J$ above the ground state, and two degenerate singlets (b, c) with excitation energy $2J$. Since for late $3d$ e_g (t_{2g}) transition metal atoms a value of $J = 0.89$ (0.72) eV has been estimated, it is very natural to assume that the latter excitations correspond to the two observed optical features near 1.5 eV. The degeneracy can be broken by non-spherical contributions and particularly by the displacement of the singlets in an antiferromagnetic background, as we show below. Note that the singlets are built from one-particle states of two different symmetries, and therefore differ from conventional ZRS. For example, in cuprates the d and p orbitals that enter the ZRS both have B_{1g} symmetry.

C. Effective model for the dynamics of the triplet-singlet excitations

Using standard perturbation theory to second-order, we construct an effective Hamiltonian that describes the AF exchange between third NN spins $S = 1$, and the movement of singlets b, c in the AF background. We neglect the singlet a whose energy is above the gap. In all perturbation processes, one of the two three-particle doublets of energy $E_3 = U + 2U' - J$ enters the intermediate state. For simplicity, we use bosonic operators b_i, c_i, t_{im} ($m = S_z$) to represent the two particle states of Eq. (2).

The result is

$$\begin{aligned}
H_{\text{eff}} = & \sum_i \left[(E_b - E_t) b_i^\dagger b_i + (E_c - E_t) c_i^\dagger c_i \right] + \\
& + \sum_{i \in A} [J_3^{(a)} \mathbf{S}_{i+\delta_1} \cdot \mathbf{S}_i + J_3^{(b)} \sum_{\delta_j \neq \delta_1} \mathbf{S}_{i+\delta_j} \cdot \mathbf{S}_i] + \\
& + h_1^c \sum_m \left(c_{i+\delta_1}^\dagger t_{im}^\dagger t_{i+\delta_1 m} c_i + \text{H.c.} \right) + \\
& + h_2^c \sum_{\delta_j \neq \delta_1} \sum_m \left(c_{i+\delta_j}^\dagger t_{im}^\dagger t_{i+\delta_j m} c_i + \text{H.c.} \right) + \\
& + h_{bc} \sum_{\delta_j \neq \delta_1} (-1)^j \sum_m \left(c_{i+\delta_j}^\dagger t_{im}^\dagger t_{i+\delta_j m} b_i + \right. \\
& \left. + b_{i+\delta_j}^\dagger t_{im}^\dagger t_{i+\delta_j m} c_i + \text{H.c.} \right), \quad (3)
\end{aligned}$$

where

$$\begin{aligned}
J_3^{(a)} &= \frac{t_1^2}{U + J}, \quad J_3^{(b)} = \frac{t_2^2 + 2t_3^2}{U + J}, \quad h_1^c = \frac{t_1^2}{U - J}, \\
h_2^c &= \frac{t_2^2 + t_3^2}{U - J}, \quad h_{bc} = \frac{t_2 t_3}{2} \left(\frac{1}{U - J} + \frac{1}{U' + J'} \right). \quad (4)
\end{aligned}$$

Taking reasonable values $U = 4$ eV, $J = 0.75$ eV, we obtain $J_3^{(a)} = 10.6$ meV, $J_3^{(b)} = 10.3$ meV, $h_1^c = 15.5$ meV, $h_2^c = 11.7$ meV, and $h_{bc} = 5.3$ meV. The first exchange interaction excluded here is due to NN hopping in the δ_1 direction, and would be of magnitude 0.55 meV. At this order of magnitude, neglected states in H_{Hub} play a role. These exchange constant are consistent with previous studies, which indicate a dominant role of third NN exchange of magnitude ~ 10 meV (17 meV in Ref. 41 using GGA+D2+U, 9 meV in Ref. 20) and larger than the NN exchange (-4 meV in Ref. 41). On the other hand, from a comprehensive comparison of neutron scattering experiments, DFT calculations, and linear spin wave predictions, it was obtained $J \simeq 13.9$ meV in Ref. 18.

H_{eff} already contains the main ingredients to describe the dynamics of the triplet-singlet excitations, including the largest spin interactions and effective hoppings. However, in order to capture some details, like the satellites observed of the lowest lying photoluminescence peak [19], one also needs to add NN exchange interactions J_1 and effective hoppings that connect the four honeycomb sublattices mentioned previously. According to the most reliable estimates, $J_1 \simeq -2.7$ meV [18] is ferromagnetic and (as expected) smaller in magnitude than the dominant third NN antiferromagnetic exchange interactions $J_3^{(a)}$ and $J_3^{(b)}$. The fact that J_1 is ferromagnetic indicates the effect of a third orbital not contained in H_{Hub} that contributes to a second-order ferromagnetic interaction through intermediate states with spin $3/2$ favoured by Hund rules.

D. Singlet dynamics in the zigzag order of NiPS₃

To study the dynamics of the singlet excitations in the antiferromagnetic order of NiPS₃, we have used an effec-

tive model $H'_{\text{eff}} = H_{\text{eff}} + H_{nn}$, where H_{eff} is described above and H_{nn} contains the NN interactions and hoppings (see Supplementary Material), *i.e.*, we work with the original structural lattice consisting of 4 honeycomb sublattices, joined by NN hoppings. For the latter, we have estimated that they are 10% of the corresponding third NN values reported above. Regarding the magnetic interactions, we have used the values obtained in Ref. [18] on the base of DFT calculations and fitting to magnetic susceptibility experiments.

In the present case, as the singlets b and c undergo hopping, eventually transforming into each other, they excite two magnons within the zigzag magnetic background. Notably, there is no direct hopping of the b singlet. Due to the lack of spherical symmetry of the system, which relaxes the relation $U' = U - 2J$ as well as equal energy of odd and even Wannier functions, the degeneracy between singlets b and c is broken. So, we impose an energy difference $E_c - E_b$ (see Eq. 3) between them, becoming the only completely free parameter in our calculation. This, along with dynamic effects, determines the energy positions of the quasi-particle peaks of the singlet spectral density functions, corresponding to the observed excitonic peaks in the optical experiments [19].

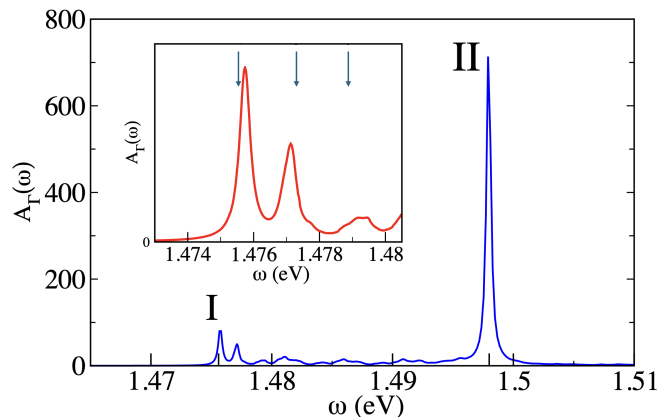


FIG. 3: (Colour online) Total spectral function of the singlets at the Γ point as a function of energy. Two quasiparticle peaks can be observed at 1.4757 and 1.498 eV, together with several satellite peaks of the first.

The position of the experimentally observed peaks is marked as I and II (see text for details). Inset: detail of the low energy peak and first satellites. The position of the experimentally observed main peak (peak I) and satellites is marked with arrows.

We have generalized the self-consistent Born approximation to compute the spectral function of the two relevant singlets of the effective model (b, c) moving in the zigzag magnetic ground state of NiPS₃. The SCBA, a reliable diagrammatic many-body method typically used to study a single hole moving in an antiferromagnetic background, was here adapted to a model with two “hole” states, each corresponding to one of the two singlets of

the effective model, exciting two magnons as they move above the antiferromagnetic order (see Supplementary Material for details of the calculation). The optimal energy difference $E_c - E_b$ that gives the results described below was found to be $E_c - E_b = 29.5$ meV, quite close to the energy difference between the peaks I and II in optical experiments [19], approximately 23 meV.

The spectral signatures of the photoluminescence and optical absorption experiments correspond to the $\mathbf{k} = \mathbf{0}$ singlet spectral functions. This is because photons have nearly zero wave vector and momentum, which enforces excitations to occur at wave vector $\mathbf{k} = \mathbf{0}$. Consequently, in Figure 3 the calculated spectral function for $\mathbf{k} = \mathbf{0}$ is displayed. The results show two quasi-particle (QP) peaks at 1.4757 and 1.498 eV, associated with singlets c and b respectively, and several replicas above the low energy peak. These QP peaks are the spectral fingerprints of singlet polaron excitations, that is, singlets coherently moving along the lattice, dressed by the magnon excitations of the zig-zag antiferromagnetic background.

The first two replicas have an energy of 1.4771 and 1.4793 eV, respectively. This is in excellent agreement with the optical experiments from Ref. 14, that observe a peak I at an energy of 1.4756 eV, a peak II at almost 1.5 eV and further replicas at 1.4773 and 1.4789 eV. The origin of the the observed widths and intensities is discussed below.

We have verified that the replicas or shoulders of the low-energy peak originate from both the two-band structure of magnon excitations (resulting from a two-spin unit cell) and the first NN hopping, that connect the four honeycomb sublattices. These shoulders are the so-called “strings”, *i.e.* the spectral representation of the singlets leaving behind a string of misaligned spins while traversing the lattice [42]. These strings are eventually repaired by quantum fluctuations of the magnetic background. The distortion of the zigzag magnetic background due to the motion of the singlets, which is much larger for the c singlet, explains the fact that the intensity is considerably lower for the low-energy singlet c than for the singlet b .

Since our calculation is performed at zero temperature, the singlet polaron peaks have zero linewidths, but they are artificially broadened by means of a small imaginary part added to the poles of the singlet self-energies. In the real system, radiative decay to the ground state should take place, broadening the higher energy peak [25, 43], as it is observed in photoluminescence experiments [14].

In Figure 4 we show the contributions of the two singlets to the spectral function of Fig. 3. We recall that singlet c , with larger hopping matrix elements [see below Eq. (4)], can hop while either transforming to a b singlet, or not. This translates into a quasi-particle peak accompanied with some shoulders or replicas, and an incoherent structure at higher energies. Moreover, the QP peak is located at an energy largely renormalized with respect to the bare energy assigned to it (1.5296 eV). On the other hand, singlet b has a spectrum that consists of

a Dirac delta-like peak centered at the bare energy of the orbital, almost 1.5 eV, indicating that this singlet does not couple to the magnetic excitations and thus behaves as a free non-interacting quasiparticle. Consequently, it is prone to the above-mentioned radiative decay. This fact naturally explains why in the experiments it appears broader than the low energy peak.

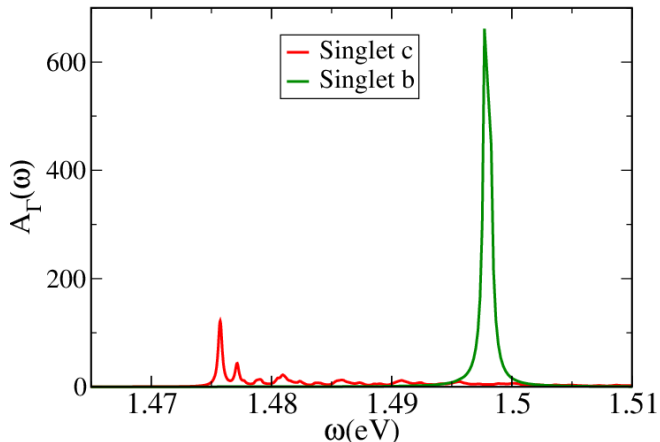


FIG. 4: (Colour online) Contribution to the spectral function of the singlets *b* and *c*.

Since these results correspond to the spectral function of the singlet excitations, it should be noted that, when comparing with optical experiments, the relative intensities of the observed peaks are affected by matrix elements. The transition from a local triplet present in the ground state to the local singlet *b* or *c* is made possible by spin-orbit coupling, and the orbital content is clearly different for both singlets. This can explain the difference in intensities between our calculation and that of the experiments.

III. DISCUSSION

Starting from maximally localized Wannier functions near the Fermi level, we have derived an effective two-band Hubbard model that accounts for key features of the spin and charge dynamics of NiPS₃. The physics is dominated by a third-neighbour hopping term between “effective” Ni states and Hund exchange, and does not require invoking a Zhang-Rice-like construction. In the strong coupling limit, the Hamiltonian reduces to the expected Heisenberg form, and naturally explains the dominant antiferromagnetic third nearest-neighbour interactions.

We caution the reader that further Wannier functions are required to elucidate additional aspects of NiPS₃ physics. For instance, the nearest-neighbor ferromagnetic interaction, albeit smaller in magnitude compared

to the primary third nearest-neighbor ones estimated in our study, necessitates a third Wannier function for a spin-3/2 intermediate state. This is likely the case also for observed d-d excitations below the charge gap [8, 25, 32], and the charge gap itself.

Using simple arguments, we establish that the sharp peaks observed in several optical experiments find a natural explanation in terms of local triplet-to-singlet excitations, which engage correlated electron states within the two Ni orbitals. Despite the absence of direct spin-light coupling, these excitations are enabled by spin-orbit coupling. The triplet-to-singlet excitations move within the Ni sublattice, distorting the spin background, giving rise to singlet polaron quasiparticles, that is, singlet states dressed by magnetic excitations.

To solve the singlet dynamics, we apply the state of the art self-consistent Born approximation. The main features of the structure observed in optical measurements—consisting of two very narrow peaks, with the low energy one having shoulders—is reproduced in our calculation, demonstrating that the origin of these peaks is due to the formation of singlet polarons as the two singlets move on the zigzag antiferromagnetic background of NiPS₃. We also explain the origin of the observed satellite peaks as strings of misaligned spins left behind by the singlet polarons as they propagate coherently on the antiferromagnetic order. Clearly, in our theory, the presence of the long-range magnetic order is essential to obtain the low-energy peak and their replicas. There is an evident connection between these ultrasharp resonances and the existence of antiferromagnetic order, as it was observed in the optical experiments [19]. Further confirmation of this picture could be provided by pump-probe time-resolved ARPES experiments, as illustrated in Ref. 44.

Although our approximation is unable to deal with a finite concentration of singlet polarons, it is reasonable to anticipate an attractive force between them. Placing two singlet polarons in proximity, (especially the low-energy *c* ones), results in an energy gain due to the diminished distortion of the background. This phenomenon mirrors the magnetic glue effect hypothesized in *t* – *J*-like models of superconductivity. Consequently, the prospect of a Bose-Einstein condensation of singlet polarons emerges as feasible.

Recent experiments have shown that the lower-energy exciton at 1.476 eV is very sensitive to the introduction of impurities [21]. This might be expected since this excitation is accompanied by a cloud of spin excitations that involves several unit cells, and it should be severely affected as the average distance between impurities is smaller than the radius of the cloud.

In conclusion, we offer a semi-quantitative explanation for the key characteristics of the remarkably narrow excitations observed below the gap in various optical experiments. These are attributed to unconventional singlet polarons: triplet-singlet excitations moving in a magnetic background. We calculate the dynamics of the singlet polarons for the first time through an advanced adaptation

of the state-of-the-art SCBA method. This allows us to identify the nature of the excited quasiparticles, which is usually a central issue in the understanding of strongly correlated systems. Our novel insights into the interplay between magnetic order and optical excitations pave the way for deeper investigations in this realm.

IV. METHODS

The DFT calculations are performed using the **Quantum Espresso** package[45], using a PAW pseudopotential within the GGA approximation as implemented by Perdew *et al.*[46]. The energy cut of the plane wave is set to 75 eV, and we use a mesh of $10 \times 8 \times 6$ points in reciprocal space. The NiPS₃ unit cell for calculations in the antiferromagnetic state consist of 4 formula units with lattice parameters $a = 5.819 \text{ \AA}$, $b = 6.621 \text{ \AA}$ and $c = 10.084 \text{ \AA}$. For the Wannierization process, we use the **Wannier90** code[47], selecting an energy region between 6.3 and 7.8 eV as marked with dashed lines in Fig. 2(a). The obtained Wannier functions are centered at Ni positions, with an excellent fit of the bands, as shown in red colour in Fig. 2(a).

The effective Hamiltonian is constructed using standard methods of perturbation theory involving degenerate states.

In order to elucidate the singlet dynamics on the zig-zag antiferromagnetic order of NiPS₃, we have applied the diagrammatic self-consistent Born approximation (SCBA) to the above mentioned effective Hamiltonian. The SCBA calculations are explained in detail in the Supplemental Material.

DECLARATIONS

- **Funding:** AAA is supported by PICT 2018-01546 and PICT 2020A-03661 of the Agencia I+D+i, Argentina. LOM is supported by CONICET under grant no. 3220 (PIP2021). IJH is supported by CONICET under grant no. 0883 (PIP2021). CSH is supported by PICT-2021-00325 of the Agencia I+D+i, Argentina. AEF is supported by the U.S. Department of Energy, Office of Science, Basic Energy Sciences under Award 476 No. DE-SC0022216
- **Competing interests:** The authors declare no competing interests
- **Authors' contributions:** C. S. Helman performed ab-initio calculations to obtain the Wannier orbitals and tight-binding parameters. A. A. Ali-gia coordinated the project, derived the many-body Hamiltonian and the effective model using perturbation theory. I. J. Hamad and L. O. Manuel carried out the SCBA calculations and wrote the supplementary material. A. E. Feiguin conceived the project and conducted calculations not included in the final version. All authors contributed equally to the analysis of the results and the preparation of the manuscript.
- **Acknowledgements:** AEF thanks Alberto de la Torre and Kemp Plumb for illuminating discussions.

-
- [1] K. Momma and F. Izumi, *Journal of Applied Crystallography* **44**, 1272 (2011).
- [2] N. D. Mermin and H. Wagner, *Phys. Rev. Lett.* **17**, 1133 (1966).
- [3] L. Savary and L. Balents, *Reports on Progress in Physics* **80** (2017), 10.1088/0034-4885/80/1/016502.
- [4] M. Gibertini, M. Koperski, A. F. Morpurgo, and K. S. Novoselov, *Nat. Nanotechnol.* **14**, 408 (2019).
- [5] J. U. Lee, S. Lee, J. H. Ryoo, S. Kang, T. Y. Kim, P. Kim, C. H. Park, J. G. Park, and H. Cheong, *Nano Lett.* **16**, 7433 (2016), arXiv:1608.04169.
- [6] K. Mehawat, A. Alfonso, S. Selter, Y. Shemerliuk, S. Aswartham, B. Büchner, and V. Kataev, *Phys. Rev. B* **105**, 214427 (2022).
- [7] T. Olsen, *J. Phys. D. Appl. Phys.* **54** (2021), 10.1088/1361-6463/ac000e, arXiv:2103.04474.
- [8] D. Afanasiev, J. R. Hortensius, M. Matthiesen, S. Mañas-Valero, M. Šiškins, M. Lee, E. Lesne, H. S. van der Zant, P. G. Steeneken, B. A. Ivanov, E. Coronado, and A. D. Caviglia, *Sci. Adv.* **7**, 1 (2021), arXiv:2010.05062.
- [9] S. Qi, D. Chen, K. Chen, J. Liu, G. Chen, B. Luo, H. Cui, L. Jia, J. Li, M. Huang, Y. Song, S. Han, L. Tong, P. Yu, Y. Liu, H. Wu, S. Wu, J. Xiao, R. Shindou, X. C. Xie, and J.-H. Chen, *Nature Communications* **14**, 2526 (2023).
- [10] C.-T. Kuo, M. Neumann, K. Balamurugan, H. J. Park, S. Kang, H. W. Shiu, J. H. Kang, B. H. Hong, M. Han, T. W. Noh, and J.-G. Park, *Scientific Reports* **6**, 20904 (2016).
- [11] K. S. Burch, D. Mandrus, and J. G. Park, *Nature* **563**, 47 (2018).
- [12] P. A. Joy and S. Vasudevan, *Phys. Rev. B* **46**, 5425 (1992).
- [13] A. R. Wildes, V. Simonet, E. Ressouche, G. J. McIntyre, M. Avdeev, E. Suard, S. A. J. Kimber, D. Lançon, G. Pepe, B. Moubaraki, and T. J. Hicks, *Phys. Rev. B* **92**, 224408 (2015).
- [14] K. Kim, S. Y. Lim, J.-U. Lee, S. Lee, T. Y. Kim, K. Park, G. S. Jeon, C.-H. Park, J.-G. Park, and H. Cheong, *Nature Communications* **10**, 345 (2019).
- [15] R. Plumley, S. Mardanya, C. Peng, J. Nokelainen, T. Assefa, L. Shen, N. Burdet, Z. Porter, A. Petsch, A. Israel-ski, H. Chen, J. S. Lee, S. Morley, S. Roy, G. Fabbri, E. Blackburn, A. Feiguin, A. Bansil, W.-S. Lee, A. Lindenberg, S. Chowdhury, M. Dunne, and J. J. Turner, "3d heisenberg universality in the van der waals antiferromag-

- net nips₃,” (2023), [arXiv:2310.07948 \[cond-mat.str-el\]](https://arxiv.org/abs/2310.07948).
- [16] M. F. DiScala, D. Staros, A. de la Torre, A. Lopez, D. Wong, C. Schulz, M. Bartkowiak, B. Rubenstein, and K. W. Plumb, “Dimensionality dependent electronic structure of the exfoliated van der waals antiferromagnet nips₃,” (2023), [arXiv:2302.07910 \[cond-mat.str-el\]](https://arxiv.org/abs/2302.07910).
- [17] T. Y. Kim and C.-H. Park, *Nano Letters* **21**, 10114 (2021).
- [18] A. Scheie, P. Park, J. W. Villanova, G. E. Granroth, C. L. Sarkis, H. Zhang, M. B. Stone, J.-G. Park, S. Okamoto, T. Berlijn, and D. A. Tennant, *Phys. Rev. B* **108**, 104402 (2023).
- [19] S. Kang, K. Kim, B. H. Kim, J. Kim, K. I. Sim, J. U. Lee, S. Lee, K. Park, S. Yun, T. Kim, A. Nag, A. Walters, M. Garcia-Fernandez, J. Li, L. Chapon, K. J. Zhou, Y. W. Son, J. H. Kim, H. Cheong, and J. G. Park, *Nature* **583**, 785 (2020).
- [20] S. Y. Kim, T. Y. Kim, L. J. Sandilands, S. Sinn, M. C. Lee, J. Son, S. Lee, K. Y. Choi, W. Kim, B. G. Park, C. Jeon, H. D. Kim, C. H. Park, J. G. Park, S. J. Moon, and T. W. Noh, *Phys. Rev. Lett.* **120**, 136402 (2018), [arXiv:1706.06259](https://arxiv.org/abs/1706.06259).
- [21] J. Kim, W. Na, J. Kim, P. Park, K. Zhang, I. Hwang, J.-W. Son, J. H. Kim, H. Cheong, and J.-G. Park, *Nano Letters* **23**, 10189 (2023).
- [22] X. Wang, J. Cao, Z. Lu, A. Cohen, H. Kitadai, T. Li, Q. Tan, M. Wilson, C. H. Lui, D. Smirnov, S. Sharifzadeh, and X. Ling, *Nature Materials* **20**, 964 (2021).
- [23] F. Dirnberger, R. Bushati, B. Datta, A. Kumar, A. H. MacDonald, E. Baldini, and V. M. Menon, *Nat. Nanotechnol.* **17**, 1060 (2022).
- [24] D. Jana, P. Kapuscinski, I. Mohelsky, D. Vaclavkova, I. Breslavetz, M. Orlita, C. Faugeras, and M. Potemski, *Phys. Rev. B* **108**, 115149 (2023).
- [25] C. J. Allington, C. A. Belvin, U. F. P. Seifert, M. Ye, T. Tai, E. Baldini, S. Son, J. Kim, J. Park, J.-G. Park, L. Balents, and N. Gedik, “Distinct optical excitation mechanisms of a coherent magnon in a van der waals antiferromagnet,” (2024), [arXiv:2402.17041 \[cond-mat.str-el\]](https://arxiv.org/abs/2402.17041).
- [26] F. C. Zhang and T. M. Rice, *Phys. Rev. B* **37**, 3759 (1988).
- [27] L. F. Feiner, J. H. Jefferson, and R. Raimondi, *Phys. Rev. B* **53**, 8751 (1996).
- [28] I. J. Hamad, L. O. Manuel, and A. A. Aligia, *Phys. Rev. Lett.* **120**, 177001 (2018).
- [29] A. A. Aligia, *Phys. Rev. B* **102**, 117101 (2020).
- [30] K. Hwangbo, Q. Zhang, Q. Jiang, Y. Wang, J. Fonseca, C. Wang, G. M. Diederich, D. R. Gamelin, D. Xiao, J.-H. Chu, W. Yao, and X. Xu, *Nature Nanotechnology* **16**, 655 (2021).
- [31] C.-H. Ho, T.-Y. Hsu, and L. C. Muhimmah, *npj 2D Materials and Applications* **5**, 8 (2021).
- [32] C. A. Belvin, E. Baldini, I. O. Ozel, D. Mao, H. C. Po, C. J. Allington, S. Son, B. H. Kim, J. Kim, I. Hwang, J. H. Kim, J. G. Park, T. Senthil, and N. Gedik, *Nat. Commun.* **12**, 6 (2021), [arXiv:2106.08355](https://arxiv.org/abs/2106.08355).
- [33] H. J. Kim and K.-S. Kim, *New Journal of Physics* **25**, 083029 (2023).
- [34] T. Klaproth, S. Aswartham, Y. Shemerliuk, S. Selzer, O. Janson, J. van den Brink, B. Büchner, M. Knupfer, S. Pazek, D. Mikhailova, A. Efimenko, R. Hayn, A. Savoyant, V. Gubanov, and A. Koitzsch, *Phys. Rev. Lett.* **131**, 256504 (2023).
- [35] J. c. v. Vučičević and M. Ferrero, *Phys. Rev. B* **109**, L081115 (2024).
- [36] J. Kim, M. Daghofer, A. H. Said, T. Gog, J. van den Brink, G. Khaliullin, and B. J. Kim, *Nature Communications* **5**, 4453 (2014).
- [37] A. A. Aligia and C. Helman, *Phys. Rev. B* **99**, 195150 (2019).
- [38] G. Pizzi, V. Vitale, R. Arita, S. Blügel, F. Freimuth, G. Géranton, M. Gibertini, D. Gresch, C. Johnson, T. Koretsune, J. Ibañez-Azpiroz, H. Lee, J.-M. Lihm, D. Marchand, A. Marrazzo, Y. Mokrousov, J. I. Mustafa, Y. Nohara, Y. Nomura, L. Paulatto, S. Poncé, T. Ponweiser, J. Qiao, F. Thöle, S. S. Tsirkin, M. Wierzbowska, N. Marzari, D. Vanderbilt, I. Souza, A. A. Mostofi, and J. R. Yates, *Journal of Physics: Condensed Matter* **32**, 165902 (2020).
- [39] A. A. Aligia and M. A. Gusmão, *Phys. Rev. B* **70**, 054403 (2004).
- [40] A. A. Aligia, *Phys. Rev. B* **88**, 075128 (2013).
- [41] B. L. Chittari, Y. Park, D. Lee, M. Han, A. H. MacDonald, E. Hwang, and J. Jung, *Phys. Rev. B* **94**, 184428 (2016).
- [42] Z. Liu and E. Manousakis, *Phys. Rev. B* **45**, 2425 (1992).
- [43] L. C. Andreani, F. Tassone, and F. Bassani, *Solid State Communications* **77**, 641 (1991).
- [44] J. Rincón, E. Dagotto, and A. E. Feiguin, *Phys. Rev. B* **97**, 235104 (2018).
- [45] P. Giannozzi, O. Andreussi, T. Brumme, O. Bunau, M. B. Nardelli, M. Calandra, R. Car, C. Cavazzoni, D. Ceresoli, M. Cococcioni, N. Colonna, I. Carnimeo, A. D. Corso, S. de Gironcoli, P. Delugas, R. A. DiStasio, A. Ferretti, A. Floris, G. Fratesi, G. Fugallo, R. Gebauer, U. Gerstmann, F. Giustino, T. Gorni, J. Jia, M. Kawamura, H.-Y. Ko, A. Kokalj, E. Küçükbenli, M. Lazzeri, M. Marsili, N. Marzari, F. Mauri, N. L. Nguyen, H.-V. Nguyen, A. O. de-la Roza, L. Paulatto, S. Poncé, D. Rocca, R. Sabatini, B. Santra, M. Schlipf, A. P. Seitsonen, A. Smogunov, I. Timrov, T. Thonhauser, P. Umari, N. Vast, X. Wu, and S. Baroni, *Journal of Physics: Condensed Matter* **29**, 465901 (2017).
- [46] J. P. Perdew, K. Burke, and M. Ernzerhof, *Phys. Rev. Lett.* **77**, 3865 (1996).
- [47] A. A. Mostofi, J. R. Yates, G. Pizzi, Y.-S. Lee, I. Souza, D. Vanderbilt, and N. Marzari, *Computer Physics Communications* **185**, 2309 (2014).